Available online at www.sciencedirect.com
ScienceDirect
Ceramics International 37 (2011) 471–479
CERAMICS INTERNATIONAL
www.elsevier.com/locate/ceramint

# The effect of the shape and size of the pores on the mechanical properties of porous HAP-based bioceramics

Dj. Veljović [a,*], R. Jančić-Hajneman [a], I. Balać [b], B. Jokić [a], S. Putić [a], R. Petrović [a], Dj. Janaćković [a]

[a] Faculty of Technology and Metallurgy, University of Belgrade, Karnegijeva 4, 11120 Belgrade, Serbia
[b] Faculty of Mechanical Engineering, University of Belgrade, Kraljice Marije 16, 11120 Belgrade, Serbia

Received 29 May 2010; received in revised form 4 July 2010; accepted 3 September 2010
Available online 29 September 2010

**Abstract**

In this study, the influence of the shape and size of the pores on the mechanical properties of the obtained porous HAP-based bioceramics was investigated. The porous HAP-based bioceramics were obtained starting from spherical calcium hydroxyapatite powder, obtained by hydrothermal syntheses. The number of shapeless inter-agglomerate pores decreased and amount of spherical intra-agglomerate pores increased on increasing the sintering temperature from 1100 °C to 1250 °C. The shape of pores also changed with thermal treatment of specimens; the small pores remained spherical while the larger pores became more spherical in shape, as was proved by image analysis. A three-dimensional, finite element unit cell model was applied to evaluate the influence of pore shape on the mechanical strength of HAP ceramics. By analyzing the effect of the shape of pores to the fracture toughness of sintered porous HAP bioceramics, it was observed that the more spherical the pores were, the tougher became the bioceramics. After sintering at 1250 °C for 2 h, measured toughness was 1.31 MPa $m^{1/2}$, which is a relatively high value for this type of bioceramics.


*Keywords:* B. Porosity; Hydroxyapatite; Fracture toughness; Finite element modeling

## 1. Introduction

Calcium hydroxyapatite (HAP, $Ca_{10}(PO_4)_6(OH)_2$), one of the most important biomaterials today, has great potential for dental, orthopedic and maxillofacial applications because of its osteoconduction, bioactivity and biocompatibility [1]. In the form of granules, porous blocks and scaffolds, sintered bioceramics based on HAP are often used in clinical practice [2,3]. Micro- and macroporous pieces have a significant role as bone substitutes [4]. The macroporosity controls access of tissues and biological fluids to the bulk of the substitute. The microporosity, on the other hand, controls the adhesion of cells and the resorption rate of the calcium phosphate. Porous materials based on HAP improve the mechanical interlock between the cells and the surface of the material and promotes osteoconductivity. The rate of integration and the volume of newly regenerated bone have been shown to be very dependent on porosity, pore size and shape [5,6].

The brittle nature of HAP and its relative poor mechanical properties, especially its low fracture toughness, limit the use of this material in load-bearing clinical applications [7,8]. Numerous efforts have been made in the development of porous bioceramics microstructures and improvement in the mechanical properties of HAP-based materials. Improvement of the fracture toughness of the HAP bioceramics is correlated to phase transformation during sintering, grain size, necks between the strong agglomerates, density and pore size, shape and roundness [9–13]. Numerous methods have been employed in order to characterize the morphology of bioceramics and to correlate it to their mechanical properties.

Image analysis, as one of the relatively new techniques, is a means of transforming visual information into quantitative data. The data obtained from image analysis are based on the shape and size of elements observed in the picture. This offers not only the observation of the structures of materials and their correlation to the properties of the materials but also examines

* Corresponding author. Tel.: +381 11 3303740; fax: +381 11 3370387.
*E-mail address:* djveljovic@tmf.bg.ac.rs (D. Veljović).

0272-8842/$36.00 
doi:10.1016/j.ceramint.2010.09.014

the state of materials during exploitation [14,15]. Finite element modeling (FEM) is a powerful tool in numerical analysis of the overall mechanical properties and stress concentration factor (SCF) in hydroxyapatite based materials [16–18]. A three-dimensional (3D) finite element (FE) unit cell model is applied to evaluate the influence of pores shape on the mechanical strength of porous HAP ceramics.

The aim of this study was to analyze the influence of microstructure (pore shape, roundness and size) on the mechanical properties of porous bioceramics based on HAP. For this purpose, spherical agglomerated HAP powder was isostatically pressed and sintered at different temperatures in order to vary the number and shape of spherical and shapeless pores. The influence of the number of spherical and shapeless pores and the roundness of the pores on the mechanical properties, mainly fracture toughness, of the obtained porous bioceramics was investigated.

## 2. Experimental

Calcium hydroxyapatite was synthesized using the modified hydrothermal method described earlier [19–21], starting from a solution of $CaCl_2{\cdot}2H_2O$ (15.96 g), $Na_2H_2EDTA{\cdot}2H_2O$ (14.8 g), $NaH_2PO_4{\cdot}2H_2O$ (12 g) and urea (12 g). The solution was heated in an autoclave at 160 °C for 3 h. Subsequently, the suspension was filtrated in a Buchner funnel, washed with warm distilled water and dried at 105 °C for 2 h.

The obtained powder was isostatically pressed at 400 MPa, for 1 min. The green compacts were sintered at 1100 °C, 1200 °C and 1250 °C for 2 h. The heating rate was 20 °C/min.

The density of the green compacts was determined by measuring the dimensions and weight, and that of sintered samples by the Archimedes method. X-ray diffraction patterns of sintered compacts were recorded using a Siemens Kristaloflex D-500, in the $2\theta$ ranging from 20° to 50°, with a scan step of 0.02°. The morphology of the powder and the sintered samples were examined using a scanning electron microscope (SEM), Jeol JSM 5800, operated at 20 keV. The obtained SEM micrographs were analyzed using software for image analysis, Image Pro Plus Program, version 4.0 for Windows.

The images were treated using appropriate filters to obtain good visibility of the pores and to enable the selection of pores for measurement. Once selected, the pores were analyzed for shape characterization using the program menu and parameters such as pore cross-section surface area, pore mean diameter, roundness and fractal dimension were determined. The present analysis was based on pore diameter and roundness as they describe in a comprehensible way the properties of interest. For each micrograph, the analysis gave data for the pore shape and size. Pore diameter was obtained as the average diameters measured at 2° intervals and passing through the centroid of the objects.

The sintered compacts were tested for indentation fracture toughness with a Buehler Indentament 1100 series, Vickers Indentation Hardness Tester, and the values of the fracture toughness were calculated using the following formula, which was derived from the model proposed by Evans and Charles [22]: $K_{Ic} = 0.0824P{\cdot}c^{-3/2}$ where $P$ is the indentation load and $c$ the length of the induced crack.

### 2.1. Finite element modeling (FEM)

To fully simulate a real microstructure, a 3D model of a random distribution of pores shape and size is required. However, a model of this size is not computationally feasible. The unit cell method reduces the complexity of the problem by assuming that the porous ceramic material is constructed of an array of basic units, each with identical composition, cell geometry and material properties (Fig. 1). A face cubic cell (FCC) is considered as a representative volume element (RVE) to simulate the real microstructures of porous ceramics (Fig. 1c). In the FCC cell, there is one spherical pore at each corner and one spherical pore in each face of the cubic cell. In other words, the random pore distribution is idealized by arranging the pores on a FCC packing.

The model is considered by introducing boundary conditions, which force the unit cell to remain in its original shape. After loading, the sides remain parallel and orthogonal, but changes in length.

This model assumes that: (1) the elastic property of the HAP ceramic is linear; (2) the ceramic is considered as an isotropic material; (3) all pores are of the same size and shape; and (4) the ceramic will not fail at the prescribed loads. For evaluation of the stress concentration factor (SCF) of different pore shapes, the unit cell (Fig. 2) is loaded in compression along the $y$-direction with adequate displacement steps. Due to the symmetry of the unit cell and the applied loads, and the use of isotropic material properties, the model was reduced to only one-eighth of the unit cell. The local coordinate system in

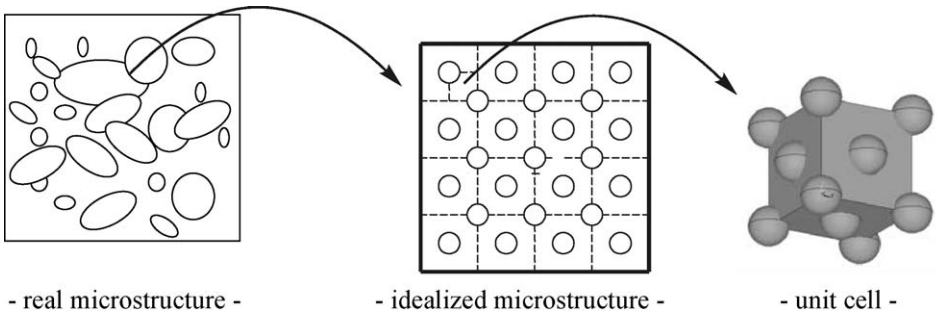


Fig. 1. Idealization of the random pore distribution, shape and size by arranging the pores on a FCC packing array.

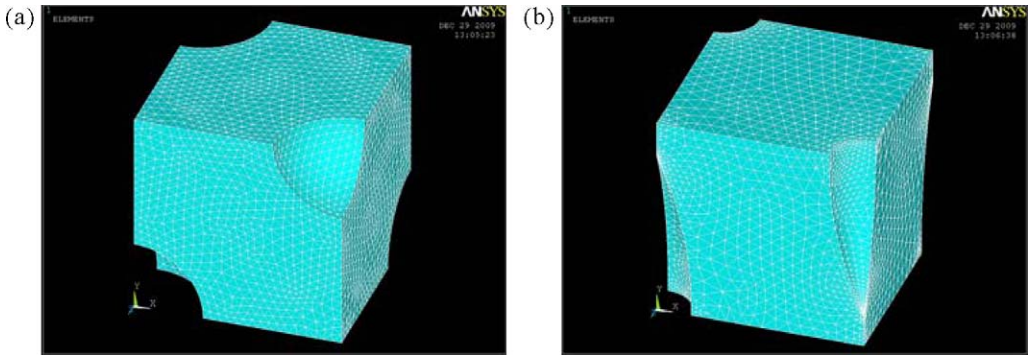


Fig. 2. (a and b) Finite element grids for spherical and crack like pores in HAP ceramic.

Fig. 2 aligns with the global one. The dimensions of this reduced unit cell are 3 μm × 3 μm × 3 μm.

All the 3D FE models were produced using ANSYS 5.7, a general-purpose finite element software package. The elements used were 10-node tetrahedral structural solid elements (with an option of 20-node solid brick elements). A representative FE grid for the evaluation of the compressive strength with PVF 0.15, shown in Fig. 2, contains 69435 elements and 97546 nodes. Each node has three degrees of freedom corresponding to the three degrees of translation. The material data used for FE analyses, adopted based on the literature data [10], where the values were around: Young's modulus $E = 100$ GPa and Poisson's ratio $\nu = 0.28$.

## 3. Results and discussion

The SEM micrograph of the calcium hydroxyapatite powder in Fig. 3 shows that spherical particles were obtained. These spherical particles are agglomerates of smaller rod-shaped nano particles below 100 nm in length. The spherical agglomerates of HAP were of relative uniform size distributions. The XRD patterns and FTIR analysis of this HAP powder, reported earlier [21], exhibited peaks and bands corresponding to calcium hydroxyapatite phase. The density of the isostatically pressed HAP green compact was $1.83 \pm 0.01$ g/cm$^3$, or 58% of the theoretical value.

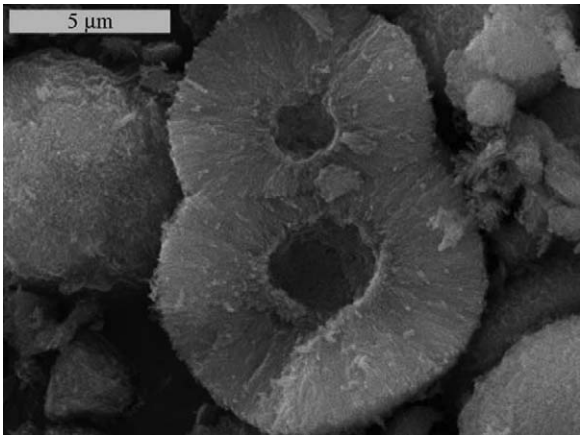


Fig. 3. SEM micrograph of the HAP powder.

The XRD patterns of the HAP1 samples sintered at 1100 °C, 1200 °C and 1250 °C (Fig. 4) show peaks suggesting that biphasic materials were obtained and that HAP was the prevailing crystalline phase. A small part of the HAP was transformed into β-TCP at 1100 °C, while the samples sintered at 1200 °C and 1250 °C consisted of HAP as the dominant crystalline phase with small amounts of α- and β-TCP.

SEM micrographs of the fracture surface of the samples sintered at 1100 °C, 1200 °C and 1250 °C for 2 h are shown in Fig. 5a–c, respectively. The SEM micrograph in Fig. 5a shows that necks between the spherical agglomerates were particularly formed at 1100 °C. Interagglomerate shapeless pores and intra-agglomerate spherical pores are evident. The density of the HAP compact sintered at 1100 °C was $2.58 \pm 0.03$ g/cm$^3$. On increasing the sintering temperature to 1200 °C, the density of the resulting HAP sample increased to $2.64 \pm 0.02$ g/cm$^3$. Fig. 5b shows that stronger necks between the spherical agglomerates were formed at 1200 °C. In addition, a higher percent of spherical pores was observed. The SEM micrograph in Fig. 5c shows that the necks between the spherical agglomerates after sintering at 1250 °C became even stronger. A large number of the interagglomerate shapeless pores disappeared, but the percent of spherical pores was even higher. The density of the HAP sample sintered at 1250 °C was $2.66 \pm 0.02$ g/cm$^3$. The porosity of the HAP sample after sintering for 2 h at

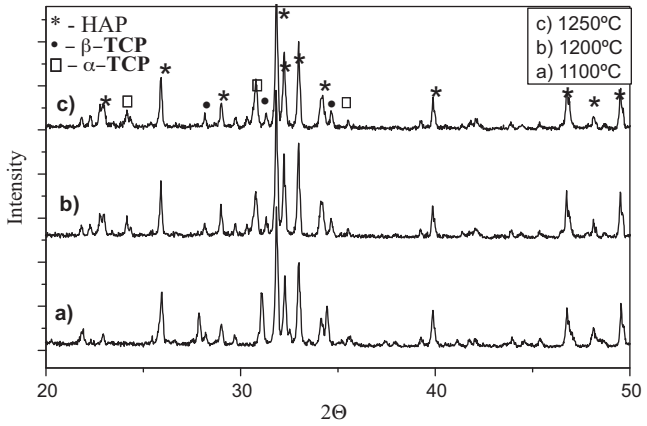


Fig. 4. XRD patterns of the HAP samples sintered at 1100 °C, 1200 °C and 1250 °C.

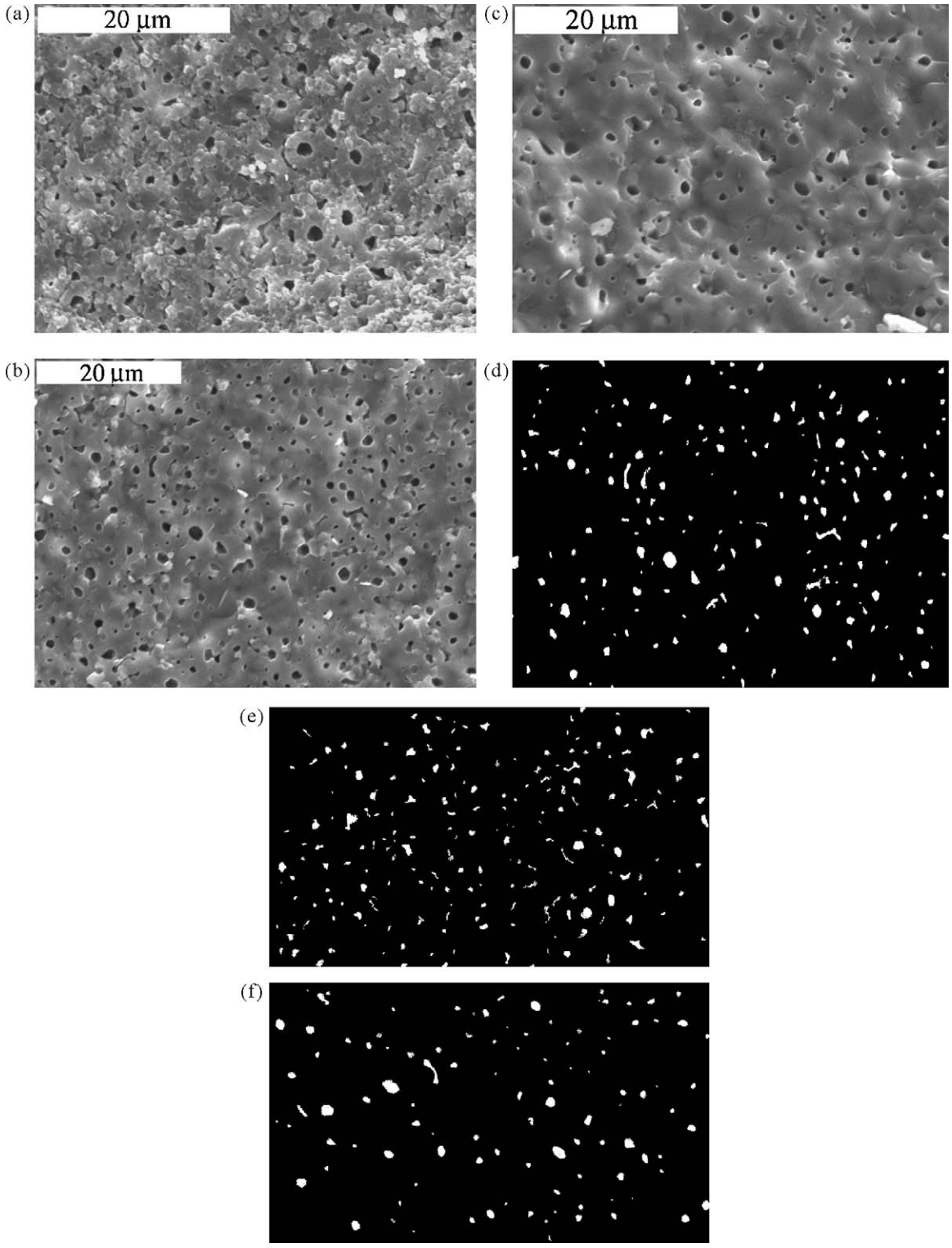


Fig. 5. SEM micrographs of a HAP samples sintered at: (a) 1100 °C, (b) 1200 °C and (c) 1250 °C for 2 h; parts of SEM micrographs, as a binary image, with pores selected for analysis (d) binary image of (a), (e) binary image of (b) and (f) binary image of (c).

1100 °C was 17.1 ± 0.2%. With increasing of the sintering temperature to 1200 °C and 1250 °C, the porosity of the samples were reduced to the values of 15.3 ± 0.3% and 14.9 ± 0.3%, respectively. The SEM micrographs at Fig. 5a–c definitely shows that the spherical intra-agglomerate pores are of stable shape in the range of temperatures of 1100–1250 °C. These visual observations were confirmed using the image analysis software.

The parts of micrographs used for image analysis are presented in Fig. 5d–f, together with the pores selected for morphology analysis, as binary images of the objects for analysis. These binary images have a clearer contrast than the

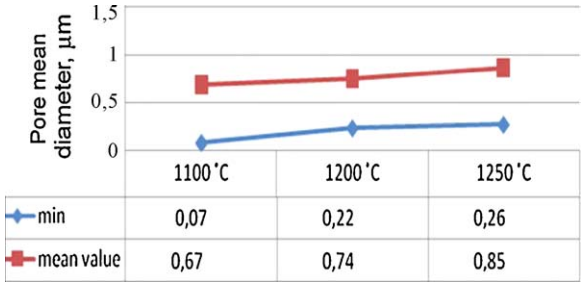


Fig. 6. The change in pore mean and minimal diameter values observed with temperature of sintering of the HAP samples.

original SEM images and are good bases for the determination of the morphology of the pores.

The analysis of the binary images gave data for the pore shape and size. The so determined values of the diameters were then analyzed using statistical tools and the mean value for all the pore diameters and minimal values of the set are presented in Fig. 6. It is obvious that the mean pore diameter increased with temperature, from around 0.68 μm to 0.85 μm. The minimal value remained relatively stable and the increase was less important as some of the small pores were of stable shape.

The pore roundness is another feature of interest. Roundness is defined as: roundness = perimeter$^2$/(4$\pi$ area). The minimal value is always 1. Fig. 7 shows that the mean value decreased mostly between the sintering temperatures 1100 °C and 1200 °C. The value of the maximal roundness also decreased with temperature, which means that with increasing sintering temperature, there are fewer pores having a complex geometry. Obviously, pores having a complex geometry are not stable and tend to change shape to spherical.

For all specimens, the same surface area was used for analysis. The number of pores observed per unit surface area decreased with temperature, as their mean cross-section surface area increased. A quantitative description of these results is presented in Fig. 8a and b.

In order to precisely define the microstructures of the samples, the roundness of pores having defined range of diameters was observed (Fig. 9). It is obvious that the small pores remained spherical at all employed sintering temperatures and that the roundness of the larger class of pores are lower, i.e. that higher is feasibility for the presence of shapeless pores with increasing of there dimension. After sintering at 1100 °C the shapeless pores larger than 3 μm were evident (Fig. 5a), while at higher temperatures their dimension were increased.

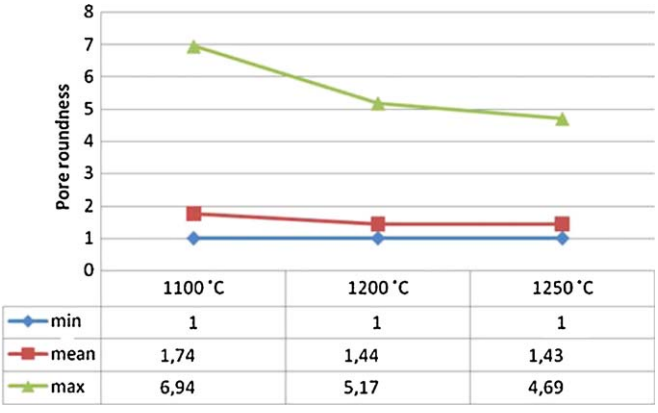


Fig. 7. Change in the mean value of the pore roundness with sintering temperature. Minimal, mean and maximal values of the pore roundness are presented.

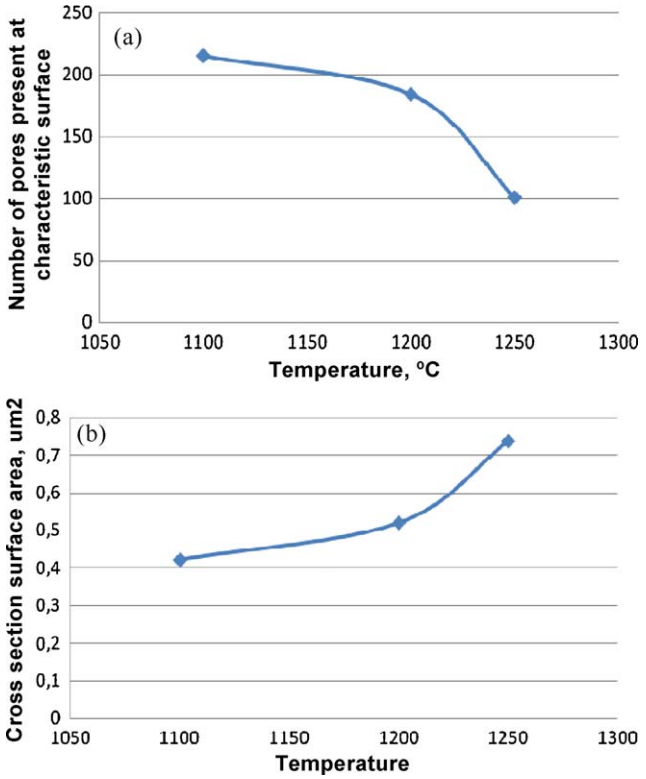


Fig. 8. Change in the number of pores at a characteristic surface and the mean pore cross-section area with temperature.

Another aspect of the data is obtained by examining the classification of the pores by roundness (Fig. 10). The round pores had a smaller diameter in all samples, obtained at different conditions, but the diameters of the non-spherical pores having a roundness larger than 1.2 were approximately same. It could be concluded that the larger pores were less spherical than the smaller ones and that the pore diameter increased for the same class of roundness with temperature. If

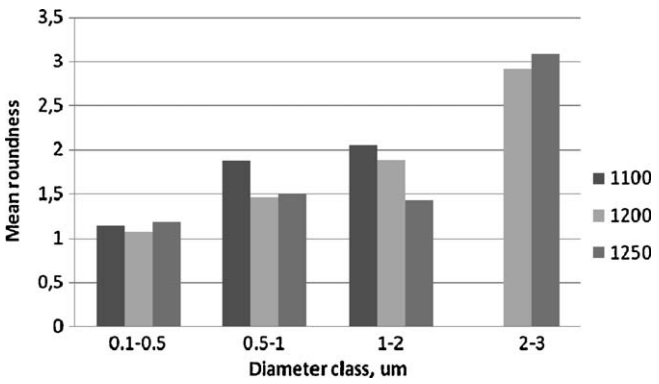


Fig. 9. The mean roundness of pores observed in specimens sintered at 1100 °C, 1200 °C and 1250 °C.

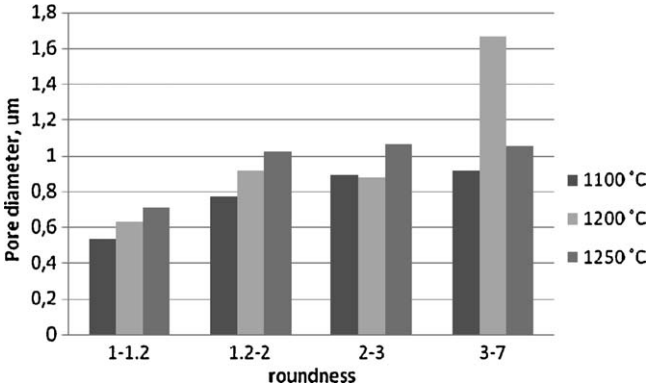


Fig. 10. Pore diameter as function of pore roundness for selected roundness classes for sintering temperatures of 1100 °C, 1200 °C and 1250 °C.

the same class of roundness for different sintering temperatures is examined then the mean diameter for the same class increases with temperature. This conclusion should be taken into account when conclusions about changes in the mechanical properties of the samples are discussed. The number and shape of pores should be considered together with crystal structure of specimens when the mechanical properties results are discussed.

The significant improvements in the fracture toughness of brittle HAP bioceramic biomaterials through control of the microstructure can be attributed to a combination of several toughening mechanisms, i.e., control of the grain size, addition of tougher particles, control of pores size and shape, etc. [6,9,10,23–26]. As can be seen from the results, the number of shapeless interagglomerate pores was reduced and amount of spherical intra-agglomerate pores increased with increasing the sintering temperature from 1100 °C to 1250 °C. According to the results of image analysis, that increasing the number of spherical pores and their roundness value convergence to 1, which corresponds to the fact that the pores become more spherical, induced an increase in the fracture toughness of the sintered porous HAP bioceramics, which was confirmed by measurement of the fracture toughness.

The images of polished surfaces of the HAP samples sintered at 1100 °C, 1200 °C and 1250 °C after the Vickers test are presented in Fig. 11a–c, respectively. These pictures demonstrate that the fracture cracks after the Vickers test of the porous sample obtained at higher temperature, with higher amounts of spherical pores, were definitely shorter.

As it is well known from fracture mechanics, a propagating crack seeks the path of least resistance (energy consumption). By applying Vickers test, during indenter loading, work (energy) performed by the applied load must be equal to the rates of change of the internal elastic energy, plastic energy and the energy spent in increasing induced cracks (where change of kinetic energy is neglected). After unloading only elastic energy is recoverable while other two are dissipated in plastic work (deformed surface) and crack growth (fracture crack). For an ideally brittle material, the energy dissipated in plastic deformation is negligible. These imply that in brittle materials (as ceramics) the amount of energy absorbed in plastic deformation is reduced to minimum extent and much more

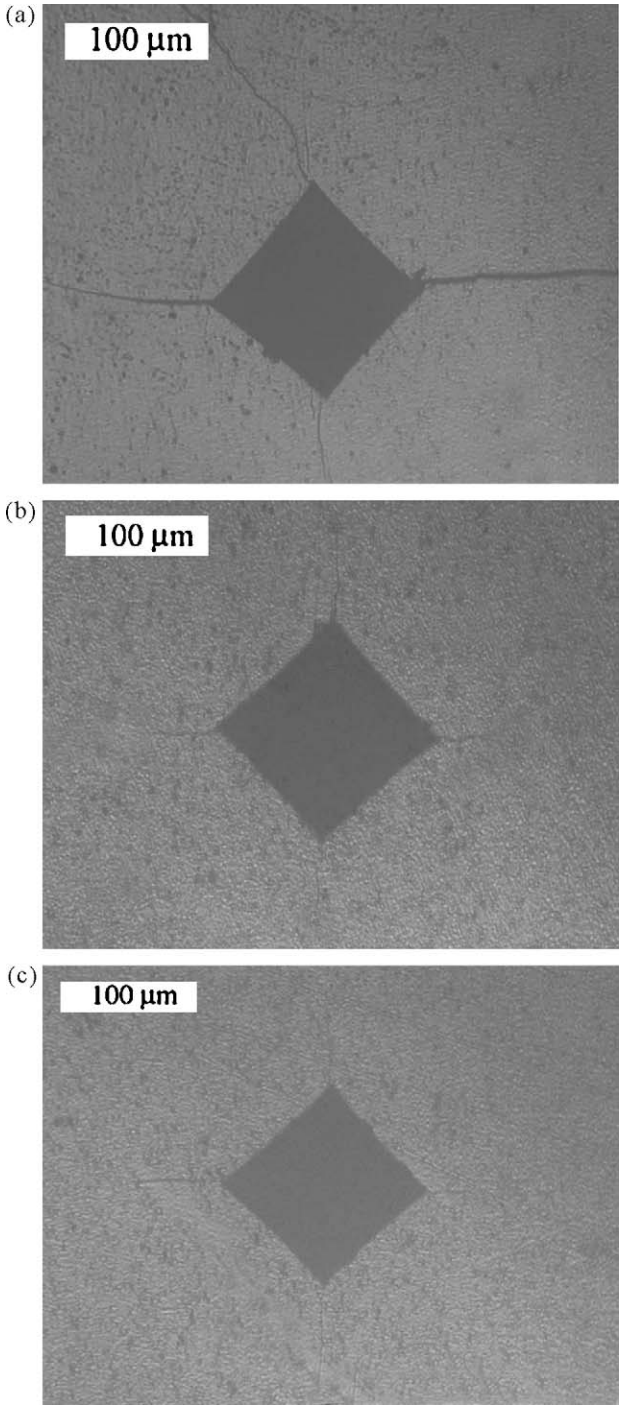


Fig. 11. (a) Image of a polished surface of a HAP samples sintered at 1100 °C after the Vickers test. (b) Image of a polished surface of a HAP samples sintered at 1200 °C after the Vickers test. (c) Image of a polished surface of a HAP samples sintered at 1250 °C after the Vickers test.

energy is thus available for fracture (crack propagation). Therefore, plastic zone at the crack tip plays an important role in energy dissipation and as well as crack growth.

The fracture toughness of the sample sintered at 1100 °C for 2 h was 1.0 MPa $m^{1/2}$. On increasing the sintering temperature to 1200 °C, the fracture toughness increased to 1.30 MPa $m^{1/2}$, but a further increase of the sintering temperature to 1250 °C did not affect an increasing of the fracture toughness, which

was practically the same as that of the sample sintered at 1200 °C. The higher critical stress intensity factor $K_{Ic}$ imply higher materials resistance to fracture.

Despite $\alpha$- and $\beta$-TCP heaving slightly higher theoretical fracture toughness than HAP, the formation of TCP phases in the HAP matrix during sintering is detrimental to the sintering and mechanical properties of the final dense and porous biphasic bioceramics [27,28,30,9,10,13]. With increasing the sintering temperature, the content of TCP phase in this kind of materials often become higher and resulted in retardation of the sintering process. Furthermore, the more intensive formation of TCP at higher temperatures influences the increasing of the grain size during the sintering, on the other side the decrease in the grain size led to an increase in the fracture toughness of the HAP based bioceramics [12,27].

Nevertheless, in the case of the HAP based materials processed in this study, the bioceramics became tougher with the increasing of sintering temperature from 1100 °C to 1250 °C till the certainly high value of $K_{Ic}$ for this kind of bioceramics. The effect of the spherical pores in the microstructure, the formation of stronger necks between the stable spherical agglomerates during the sintering and increase in the density of the sintered materials, could be the reasons for the appreciably higher fracture toughness of this type of bioceramics. These imply that in this case crack needs higher amount of energy for propagation. As can be seen from the results, the fracture toughness was directly related to the type of porosity. The higher percent of spherical pores at the fracture surface of the compact sintered at the higher temperature could be the main reason for the increase of the fracture toughness. The effect of spherical interagglomerate pores on the fracture toughness of the porous bioceramics is a decrease in crack growth, which would create a highly cranky pathway and a corresponding increase in the dissipation of energy during crack propagation [6,13]. Since the amount of energy available for crack propagation is limited, this implies better toughness properties in this type of material.

From the SEM micrograph in Fig. 12a, it can be seen that the crack propagated until it met strong sintered spherical agglomerate with the spherical intra-agglomerate pore, made devious crack and then continued. The formation of continuous and strong necks between the spheres, and strong nature of these spherical agglomerates, could be the main reason for increased fracture toughness (Fig. 12b).

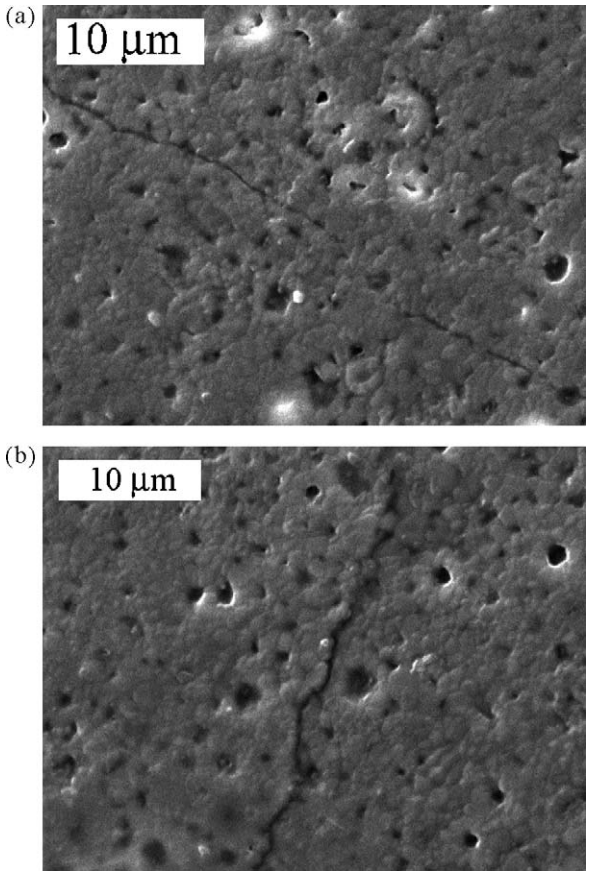


Fig. 12. (a and b) Cracks in HAP samples sintered at 1200 °C after the Vickers test.

In general, the fracture toughness values for most HAP samples reported in the literature varied between 0.60 and around 1 MPa $m^{1/2}$. The indentation fracture toughness of the HAP compacts obtained in this study was appreciably higher than those reported in many studies for porous and dense HAP ceramics [19,29–31].

The FEM results shown in Fig. 13 confirmed the observed improved mechanical strength of porous HAP ceramics with spherical pores compared with other pore shapes. The shape and Von Mises stress contours of the deformed ceramic, shown

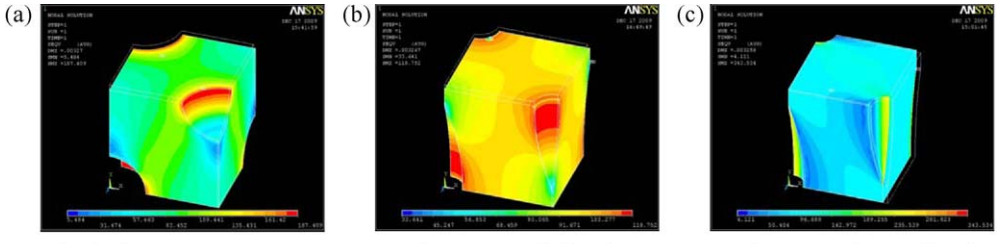


Fig. 13. (a–c) Von Mises stress distribution in the HAP ceramics for 0.155 PVF (the stress values are in $\mu N/\mu m^2$ = MPa) with calculated values of the SCF.

in Fig. 13, were achieved by loading the grid shown in Fig. 2 with a prescribed displacement in the $y$-direction of the nodes positioned at the upper surface of the cube ($y = 3$ μm). In order to extend the uniaxial stress information to the multiaxial stress state, the Von Mises equivalent stress is presented.

The nominal stress ($\sigma_{nom}$) was determined by summing the reactions on the constrained surface opposite the loaded surface and dividing by the area ($A = 9$ μm$^2$). The side surfaces remain parallel to their original directions. The stress values, shown in Fig. 13, are the result of loading which corresponds to an applied strain of 0.1%.

The SCF presents the ratio of the maximum stress to the nominal applied stress (SCF = $\sigma_{max}/\sigma_{nom}$). The SCF is directly proportional to the mechanical strength. The level of the SCF for porous HAP with a porosity of 15% ranged from a value of 3.84 for crack-like pores aligned orthogonally to the load direction to 1.25 for crack pores with the array parallel to the load direction, while the calculated value of the SCF was 2.21 for spherical pores. Bearing in mind that it is impossible to obtain an array in which non-spherical pores are aligned parallel to the load, these results suggest that porous HAP with sphere-like pore shapes generates lower values of the SCF and therefore better strength properties compared to crack-like pore shapes.

The region of the pores where the maximum stress ($\sigma_{max}$) occurs is in certain circumstances the favorable place for local flaw deformation as well as crack initiation and propagation. From this point of view porous material with sphere-like pores has more resistance to fracture than material with crack-like pore shapes.

## 4. Conclusions

Porous HAP-based bioceramics was obtained starting from spherical calcium hydroxyapatite powder, obtained by hydrothermal syntheses. The microstructures of the obtained porous bioceramics were characterized by spherical intra-agglomerate pores and shapeless interagglomerate pores. On increasing the sintering temperature from 1100 °C to 1250 °C, the number of shapeless interagglomerate pores was certainly reduced and the percent of spherical intra-agglomerate pores become higher. From the results of the determination of the pore morphology, it could be concluded that with increasing temperature, the number of pores decreased as their individual volume increased; hence, a structure having a smaller number of larger pores was obtained. The shape of the pores also changed with increasing temperature; the small pores remained spherical and the larger pores became more spherical.

According to the results that increasing of amount of spherical pores and decreasing their roundness value, which corresponds to the pores becoming more spherical, induced an increase in the fracture toughness of sintered porous HAP bioceramics. The fracture toughness of this type of bioceramics was directly related to the type of porosity. The higher amount of spherical pores at the fracture surface of the compacts sintered at higher temperatures and the formation of continuous necks between the strong spherical agglomerates could be the reason for the increased fracture toughness.

Controlled porous HAP-based bioceramics materials with different porosities may be produced by this method by varying the size of the starting spherical agglomerates of the HAP powders. FEM analysis confirmed that porous HAP with sphere-like pores has better strength properties compared to non-spherical pore shapes.

The controlled morphology and this kind of porous microstructure, due to the necessary biological function of porosity, together with the good mechanical properties of these bioceramic materials could be one of the key increments for successful implants.

## Acknowledgements

The authors wish to acknowledge the financial support from the Ministry of Science and Technological Development of the Republic of Serbia through the projects 142070B and EUREKA E! 3033 Bionanocomposite.

## References

[1] L.L. Hench, Bioceramics: from concept to clinic, J. Am. Ceram. Soc. 74 (1991) 1487–1510.
[2] J. Chevalier, L. Gremillard, Ceramics for medical applications: a picture for the next 20 years, J. Eur. Ceram. Soc. 29 (2009) 1245–1255.
[3] E.C. Shors, R.E. Holmes, Porous hidroxyapatite, in: L.L. Hench, J. Wilson (Eds.), An Introduction to Bioceramics, World Scientific, Singapore, 1993 , pp. 181–198.
[4] R. Vani, E.K. Girija, K. Elayaraja, S.P. Parthiban, R. Kesavamoorthy, S.N. Kalkura, Hydrothermal synthesis of porous triphasic hydroxyapatite/(α and β) tricalcium phosphate, J. Mater. Sci.: Mater. Med. (2009), doi:10.1007/s10856-008-3480-8.
[5] M. Kawata, H. Uchida, K. Itatani, I. Okada, S. Koda, M. Aizawa, Development of porous ceramics with well-controlled porosities and pore sizes from apatite fibers and their evaluations, J. Mater. Sci.: Mater. Med. 15 (2004) 817–823.
[6] R. Kumar, K.H. Prakash, P. Cheang, K.A. Khor, Microstructure and mechanical properties of spark plasma sintered zirconia-hydroxyapatite nano-composite powders, Acta Mater. 53 (2005) 2327–2335.
[7] J.E. Barralet, S. Best, W. Bonfield, Effect of sintering parameters on the density and microstructure of carbonate hydroxyapatite, J. Mater. Sci.: Mater. Med. 11 (2000) 719–724.
[8] C.C. Ribeiro, C.C. Barrias, M.A. Barbosa, Preparation and characterization of calcium-phosphate porous microspheres with a uniform size for biomedical applications, J. Mater. Sci.: Mater. Med. 17 (2006) 455–463.
[9] Dj. Veljovic, B. Jokic, R. Petrovic, E. Palcevskis, A. Dindune, I.N. Mihailescu, Dj. Janackovic, Processing of dense nanostructured HAP ceramics by sintering and hot pressing, Ceram. Int. 35 (2009) 1407–1413.
[10] C.Y. Tang, P.S. Uskokovic, C.P. Tsui, Dj. Veljovic, R. Petrovic, Dj. Janackovic, Influence of microstructure and phase composition on the nanoindentation characterization of bioceramic materials based on hydroxyapatite, Ceram. Int. 35 (2009) 2171–2178.
[11] O. Prokopiev, I. Sevostianov, Dependence of the mechanical properties of sintered hydroxyapatite on the sintering temperature, Mater. Sci. Eng. A 31 (2006) 218–227.
[12] Dj. Veljovic, I. Zalite, E. Palcevskis, I. Smiciklas, R. Petrović, Dj. Janackovic, Microwave sintering of fine grained HAP and HAP/TCP bioceramics, Ceram. Int. 36 (2010) 595–603.
[13] Dj. Veljović, E. Palcevskis, A. Dindune, S. Putić, I. Balać, R. Petrović, Dj. Janackovic, Microwave sintering improves the mechanical properties of biphasic calcium phosphates from hydroxyapatite microspheres produced from hydrothermal processing, J. Mater. Sci. 45 (12) (2010) 3175–3183.

[14] M. Posarac, M. Dimitrijevic, T. Volkov-Husovic, J. Majstorovic, B. Matovic, The ultrasonic and image analysis method for non-destructive quantification of the thermal shock damage in refractory specimens, Mater. Des. 30 (2009) 3338–3343.
[15] M.S. Djošic, V.B. Miškovic-Stankovic, Z.M. Kačarevic-Popovic, B.M. Jokic, N. Bibic, M. Mitric, et al., Electrochemical synthesis of nanosized monetite powder and its electrophoretic deposition on titanium, Colloids Surf. A 341 (2009) 110–117.
[16] I. Balać, P.S. Uskoković, N. Ignjatović, R. Aleksić, D. Uskoković, Stress analysis in hydroxyapatite/poly-L-lactide composite biomaterials, Comput. Mater. Sci. 20 (2001) 275–283.
[17] I. Balać, P.S. Uskoković, R. Aleksić, D. Uskoković, Predictive modeling of the mechanical properties of particulate hydroxyapatite reinforced polymer composites, J. Biomed. Mater. Res. 3 (2002) 793–799.
[18] I. Balać, M. Milovančević, C.Y. Tang, P.S. Uskoković, D. Uskoković, Estimation of the elastic properties of a particulate polymer composite using a face-centered cubic FE model, Mater. Lett. 8 (2004) 2437–2441.
[19] Y. Fujishiro, T. Sato, A. Okuwaki, Coating of hydroxyapatite on metal plates using thermal dissociation of calcium-EDTA chelate in phosphate solutions under hydrothermal conditions, J. Mater. Sci. 6 (1995) 172–176.
[20] Dj. Janaćkovic, I. Petrovic-Prelevic, Lj. Kostic-Gvozdenovic, R. Petrovic, V. Jokanovic, D. Uskokovic, Influence of synthesis parameters on the particle sizes of nanostructured calcium-hydroxyapatite, Key Eng. Mater. 203 (2001) 192–195.
[21] B. Jokic, I. Jankovic-Castvan, Dj. Veljović, D. Bucevac, K. Obradovic-Djuricic, R. Petrovic, Dj. Janackovic, Synthesis and settings behavior of α-TCP from calcium deficient hyroxyapatite obtained by hydrothermal method, J. Opto. Adv. Mater. 9 (2007) 1904–1910.
[22] A.G. Evans, E.A. Charles, Fracture toughness determinations by indentation, J. Am. Ceram. Soc. 59 (1976) 371–372.
[23] Y.M. Chiang, D.P. Birnie, W.D. Kingery, Physical Ceramics, John Wiley and Sons, New York, 1997.
[24] B.R. Lawn, D.B. Marshall, Hardness, toughness and brittleness: an indentation analysis, J. Am. Ceram. Soc. 62 (1979) 347–350.
[25] P.V. Landuyt, F. Li, J.P. Keustermans, J.M. Streydio, F. Delannay, E. Munting, The influence of high sintering temperatures on the mechanical properties of hydroxyapatite, J. Mater. Sci.: Mater. Med. 6 (1995) 8–13.
[26] W.D. Callister, Materials Science and Engineering an Introduction, John Wiley and Sons, New York, 2003.
[27] S. Raynaud, E. Champion, D. Bernache-Assollant, Calcium phosphate apatites with variable Ca/P atomic ratio II. Calcination and sintering, Biomaterials 23 (2002) 1073–1080.
[28] R.Z. Legeros, S. Lin, R. Rohanizadeh, D. Mijares, J.P. Legeros, Biphasic calcium phosphate bioceramics: preparation, properties and applications, J. Mater. Sci.: Mater. Med. 14 (2003) 201–209.
[29] A. Banerjee, A. Bandyopadhyay, S. Bose, Hydroxyapatite nanopowders: synthesis, densification and cell–materials interaction, Mater. Sci. Eng. C 27 (2007) 729–735.
[30] S. Raynaud, E. Champion, J.P. Lafon, D. Bernache-Assollant, Calcium phosphate apatites with variable Ca/P atomic ratio III. Mechanical properties and degradation in solution of hot pressed ceramics, Biomaterials 23 (2002) 1081–1089.
[31] G. Muralithran, S. Ramesh, The effects of sintering temperature on the properties of hydroxyapatite, Ceram. Int. 26 (2000) 221–230.